university of groningen

University Medical Center Groningen

University of Groningen

Eighty-Eight Percent Directional Guiding of Spin Currents with 90 mu m Relaxation Length in Bilayer Graphene Using Carrier Drift

Ingla-Aynes, Josep; Meijerink, Rick J.; van Wees, Bart J.

Published in:
Nano Letters

DOI:
10.1021/acs.nanolett.6b01004

IMPORTANT NOTE: You are advised to consult the publisher's version (publisher's PDF) if you wish to cite from it. Please check the document version below.

Document Version
Publisher's PDF, also known as Version of record

Publication date:
2016

Link to publication in University of Groningen/UMCG research database

Citation for published version (APA):
Ingla-Aynes, J., Meijerink, R. J., & van Wees, B. J. (2016). Eighty-Eight Percent Directional Guiding of Spin Currents with 90 mu m Relaxation Length in Bilayer Graphene Using Carrier Drift. *Nano Letters*, *16*(8), 4825-4830. https://doi.org/10.1021/acs.nanolett.6b01004

Copyright
Other than for strictly personal use, it is not permitted to download or to forward/distribute the text or part of it without the consent of the author(s) and/or copyright holder(s), unless the work is under an open content license (like Creative Commons).

The publication may also be distributed here under the terms of Article 25fa of the Dutch Copyright Act, indicated by the “Taverne” license. More information can be found on the University of Groningen website: https://www.rug.nl/library/open-access/self-archiving-pure/taverne-amendment.

Take-down policy
If you believe that this document breaches copyright please contact us providing details, and we will remove access to the work immediately and investigate your claim.

Downloaded from the University of Groningen/UMCG research database (Pure): http://www.rug.nl/research/portal. For technical reasons the number of authors shown on this cover page is limited to 10 maximum.

NANO LETTERS
Letter
pubs.acs.org/NanoLett

Eighty-Eight Percent Directional Guiding of Spin Currents with 90 μm Relaxation Length in Bilayer Graphene Using Carrier Drift

Josep Ingla-Aynés,* Rick J. Meijerink, and Bart J. van Wees

Physics of Nanodevices, Faculty of Mathematics and Natural Sciences, Zernike Institute for Advanced Materials, University of Groningen, Groningen 9747 AG, The Netherlands

Supporting Information

Downloaded via UNIV GRONINGEN on April 1, 2019 at 09:39:09 (UTC).
See https://pubs.acs.org/sharingguidelines for options on how to legitimately share published articles.

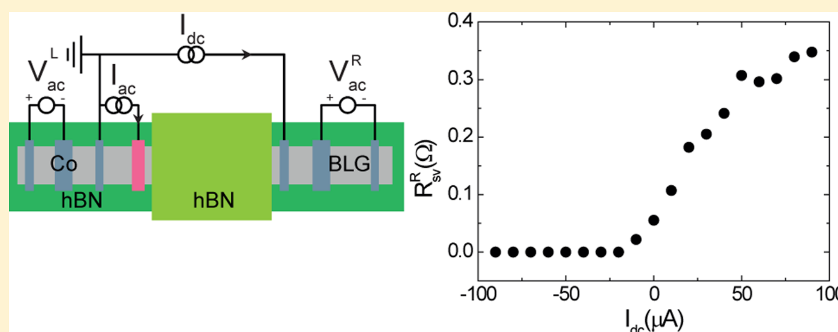

ABSTRACT: Electrical control of spin signals and long distance spin transport are major requirements in the field of spin electronics. Here, we report the efficient guiding of spin currents at room temperature in high mobility hexagonal boron nitride encapsulated bilayer graphene using carrier drift. Our experiments, together with modeling, show that the spin relaxation length, that is 7.7 μm at zero bias, can be tuned from 0.6 to 90 μm when applying a DC current of $\mp$90 μA, respectively. Our results also show that we are able to direct spin currents to either side of a spin injection contact. Eighty-eight percent of the injected spins flows to the left when I_{dc} = −90 μA and eighty-two percent flows to the right when the drift current is reversed. These results show the potential of carrier drift for spin-based logic operations and devices.

KEYWORDS: *graphene, boron nitride, spin transport, drift*

Propagation of spins has been traditionally studied using spin diffusion, which is a slow, non directional process that limits the range over which spins can be transported without losing the spin polarization. In contrast, transport induced by carrier drift allows for fast and directional propagation of spins enabling long distance spin transport.[1] This effect relies on the fact that a charge current is associated with an in-plane electric field E, causing carriers to drift with a velocity $v_d = \mu E$ which is proportional to the electronic mobility μ of the channel. As a result, when a spin accumulation is present, the propagation of spins can be controlled with a drift field.[2,3] Low temperature spin drift experiments performed in semiconductors such as silicon[4−6] and gallium arsenide[7] showed a modulation of the Hanle spin precession with the applied bias. Room temperature modulation of the spin relaxation length between 0.85 and 4.53 μm was obtained for Si.[6] Spin signals have been measured over 350 μm in Si for temperatures up to 150 K.[8]

Graphene is a 2D material that presents outstanding electronic properties[9,10] and long spin relaxation times[11−13] that are ideal for spintronic applications.[14,15] Graphene's unprecedentedly high electronic mobilities μ are an attractive incentive for spin drift measurements. Reference 16 represents the proof of principle for this effect in graphene on SiO_2 at room temperature. However, the efficiency was limited by the low mobility and short spin relaxation time of the graphene samples on SiO_2. In the past years, several approaches have been used to enhance the electronic quality of graphene. In particular, the use of hexagonal boron nitride (hBN) as a substrate has led to a great improvement of the graphene quality in terms of charge[17,18] and spin transport.[19−22]

In this Letter, we show that the magnitude of the spin signal can be controlled efficiently by applying drift currents in high mobility hBN encapsulated bilayer graphene (BLG). In particular, at V_{bg} = −13.75 V, the nonlocal resistance is enhanced by more than 500% applying a drift current of 90 μA. By reversing the drift current, the spin signal is suppressed below the noise level, that is less than 10% of its zero drift value, for I_{dc}< −20 μA. These results, together with a model that accounts for drift in our geometry, show that we have achieved a strong modulation of the spin relaxation length from 0.6 to 90 μm when applying a moderate DC drift current (I_{dc}) of ±90 μA.

Also, we demonstrate the efficiency of a drift field in directing the spin currents, showing that we can steer the injected spin currents to the right and left sides of the injecting contact with

Received: March 8, 2016
Revised: July 8, 2016
Published: July 11, 2016

ACS Publications © 2016 American Chemical Society

DOI: 10.1021/acs.nanolett.6b01004
Nano Lett. 2016, 16, 4825−4830

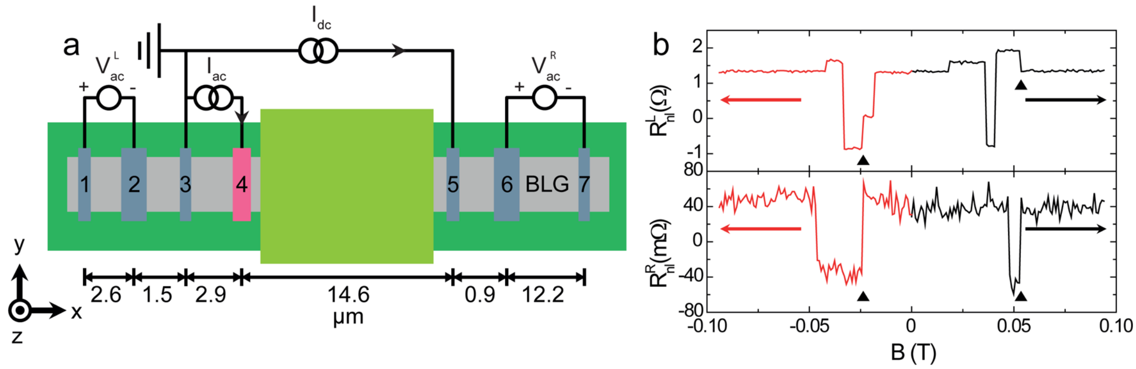

Figure 1. (a) Measurement geometry. The hBN/bilayer graphene/hBN stack is placed on a n^{+2} doped Si/SiO_2 substrate and the ferromagnetic contacts are made on the nonencapsulated regions. An AC current (I_{ac}) is sent between contacts 4 and 3 to create a spin imbalance and a DC current (I_{dc}) is sent between 5 and 3 to induce drift. The signal is detected simultaneously in the left side of the injection circuit and across the encapsulated region ($V_{ac}^{L(R)}$ respectively). Two more contacts are present between 3 and 4 but are not shown in the sketch for simplicity. (b) Nonlocal resistances in the left and right detection circuits (top and bottom panels, espectively) as a function of an in-plane magnetic field at I_{dc} = 0 μA. Backgrounds of −5.5 and 4.85 Ω respectively have been subtracted for clarity. The arrows indicate the magnetic field sweep direction and the triangles the switches caused by the magnetization reversal of contact 4.

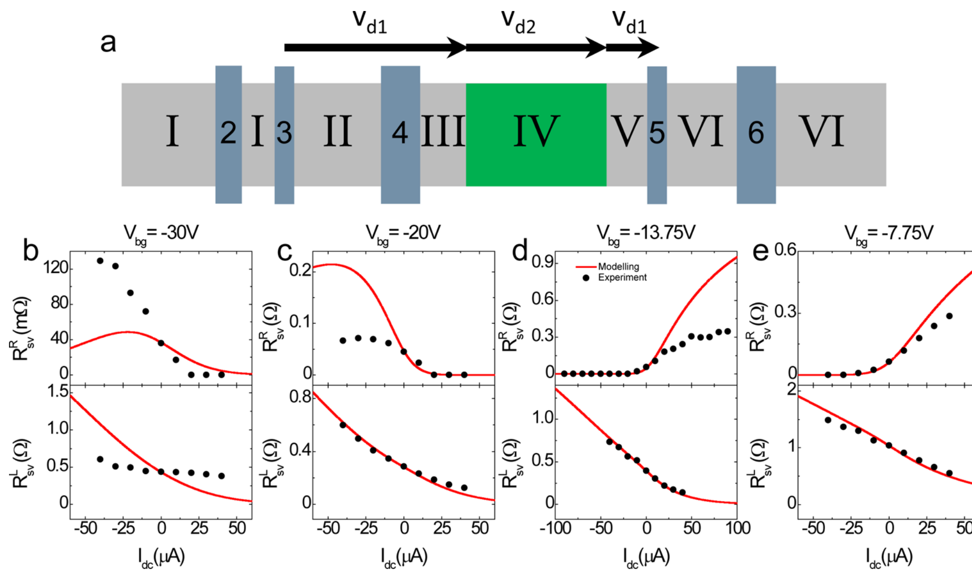

Figure 2. (a) Sketch of the simulated device with four different regions. I, II, III, V, and VI are the nonencapsulated regions and are assumed to have the same transport properties. IV is the encapsulated region and drift is considered in regions II, III, IV, and V with drift velocities v_{d1} and v_{d2}. The graphene is assumed to be infinite at both left and right sides. (b)−(e) Measured amplitude of the spin signal generated by contact 4 in the detectors 6 (top panels) and 2 (bottom panels) at V_{bg} = −30, −20, −13.75, and −7.75 V, respectively. The red curves are obtained from modeling and using the parameters extracted from independent measurements.

efficiencies of 88% and 82% by applying drift currents of ∓90 μA, respectively.

When applying a drift field in the graphene channel, the spin accumulation follows the drift diffusion equation

$$D_s \frac{d^2 n_s(x)}{dx^2} - v_d \frac{dn_s(x)}{dx} - \frac{n_s(x)}{\tau_s} = 0 \quad (1)$$

where D_s is the spin diffusion coefficient, n_s the spin accumulation, τ_s the spin relaxation time and $v_d = -(+)\mu E$ when the carriers are electrons (holes). As can be seen from eq 1, when an electric field is applied, the propagation of spin signals is no longer symmetric in the ± x direction. This equation has solutions in the form of $n_s = A\exp(x/\lambda_+) + B\exp(-x/\lambda_-)$ where $\lambda_{+(-)}$ is the relaxation length for spins propagating toward the left (right) in our system (also called upstream (downstream) in the literature[2])

$$\frac{1}{\lambda_\pm} = \pm\frac{v_d}{2D_s} + \sqrt{\left(\frac{1}{\sqrt{\tau_s D_s}}\right)^2 + \left(\frac{v_d}{2D_s}\right)^2} \quad (2)$$

This asymmetry in the spin propagation allows us to direct the spin currents in a controlled way. Because $E = I_{dc}R_{sq}/W$ where R_{sq} is the square resistance and W the width of the channel, such control can be achieved using I_{dc} with an efficiency that is given by the applied electric field and the mobility of the device.

Our results are obtained using a bilayer graphene device that is partially encapsulated between two hBN flakes in the geometry shown in Figure 1a and prepared using a dry transfer technique.[18,23] The bilayer graphene obtained by exfoliation is supported by a bottom hBN flake (23 nm thick) and the ferromagnetic Co contacts (0.8 nm TiO_x/65 nm Co/5 nm Al) with widths ranging from 0.15 to 0.55 μm are placed on the outer regions. The central region is encapsulated between both

DOI: 10.1021/acs.nanolett.6b01004
Nano Lett. 2016, 16, 4825−4830

bottom and top hBN (21 nm thick) that is covered by a top gate (not shown for clarity) which we have set to zero voltage relative to contact 4. The spin and charge transport properties of this sample at room temperature and 4 K can be found in ref 21.

We send an AC current (I_{ac}) of 1 μA between contacts 4 and 3 to inject spins. The in-plane electric field is applied by sending I_{dc} between contacts 5 and 3. We have not applied any DC bias to contact 4 to keep its injection efficiency constant.[24] We have used the standard low frequency lock-in technique to detect the AC spin signals (13 Hz) between contacts 2 and 1 and 6 and 7 simultaneously to study the effect of a drift current on the spin signal. When applying a magnetic field in the y direction, the contact magnetizations are controlled independently due to their different width that gives rise to different coercive fields. The results for the nonlocal spin signals are shown in Figure 1b. Here, the nonlocal voltage is normalized by I_{ac} to obtain the nonlocal resistance in the left (right) side of the injector: $R_{nl}^{L(R)} = V_{ac}^{L(R)}/I_{ac}$ where $V_{ac}^{L(R)}$ is the voltage measured between contacts 2 and 1 (6 and 7).

In Figure 1b, at B$\approx$ −25 mT and 55 mT we see simultaneous switching in R_{nl}^{R} and R_{nl}^{L} indicated with black triangles. Because no other switches occur simultaneously in both measurements, we attribute these switches to contact 4 that is our spin injector contact of interest.[25] We define the spin signal created by spin injection by contact 4: $R_{sv}^{L(R)} = \Delta R_{nl}/2$ where $\Delta R_{nl}^{L(R)}$ is the change in the nonlocal resistance in the left (right) detector caused by a switch of contact 4.

The carrier density of the BLG can be modified using the backgate,[26] formed in our case by the n^{++} doped Si substrate and the 300 nm thick SiO_2 and 23 nm thick hBN gate insulators. In Figure 2b−e we show the spin signal dependence on the drift current at four different gate voltages (−30 V, −20 V, −13.75 V and −7.75 V respectively) corresponding to carrier densities of -1.1×10^{12}, -2.1×10^{11}, 3.3×10^{11}, and 8.6×10^{11} cm^{-2} in the encapsulated regions. These are chosen to show the effect of drift under the most relevant gating conditions. The encapsulated region can be electron and hole-doped at different carrier densities around the charge neutrality point (V_{bg} = −17.5 V). The outer regions are highly doped and the charge neutrality point is around −50 V, hence the carriers are electrons for all the gate voltages.

When the encapsulated and nonencapsulated regions are both electron doped the spin signals measured at both detectors show an opposite trend with respect to I_{dc} (Figure 2d,e). This can be understood taking into account that the detectors are at opposite sides of the injector contact and the carriers (electrons in both regions) are pushed toward the right (left) for positive (negative) drift velocities enhancing (reducing) the spin signal in the right (left) detector. The control of the spin signal across the encapsulated region (right detector) is very efficient: At $I_{dc} < -20$ μA the spin signal is suppressed below the noise level (5 mΩ), whereas the signal is enhanced by more than 500% applying I_{dc} = 90 μA at V_{bg} = −13. 75 V and 300% applying I_{dc} = 40 μA at V_{bg} = −7. 75 V. In the left detector, the modulation is dominated by the drift in the nonencapsulated region and the spin signal changes less strongly with the drift current.

In Figure 2b and c the carriers in the inner and outer regions have opposite polarity. In this case, the spin signals at both sides of the injector increase for negative I_{dc}. This is because electrons and holes react in opposite ways when an electric field is created by I_{dc}. In this case, the modulation of the spin signal across the encapsulated region is less efficient. It increases by 60% (200%) for negative I_{dc} and it is suppressed below the noise level for $I_{dc} > 20$ μA at V_{bg} = −20 V (−30 V). We explain the smaller increase taking into account that, in this configuration and when applying a negative I_{dc}, the electric field pulls the spins away from the injector (contact 4) in both directions and the spin accumulation below the injector decreases in a more pronounced way than at V_{bg} = −13.75 and −7.75 V. Since the outer regions are electron-doped in the whole range, R_{nl}^{L} decreases with increasing drift currents for all the values.[27]

To understand the spin current distribution in the channel, we have adapted the model developed in ref 28 to the geometry shown in Figure 2a. Region IV (green) is encapsulated, whereas the other ones are not. We account for the electric field applied in regions II, III, IV, and V using the drift diffusion eq (eq 1). Regions III and V are 0.5 μm long and the spacing between contacts is the one described in Figure 1a.

To extract the parameters needed for this model we have performed a similar analysis as in 19 and 21. The spin relaxation time in the nonencapsulated regions I, II, III, V, and VI in Figure 2a is extracted from Hanle precession measurements carried out in region I. The spin relaxation time in the encapsulated region is extracted using the three regions model derived in ref 29. For this purpose, we have calculated Hanle precession across the encapsulated region IV and used the transport parameters of both encapsulated and nonencapsulated regions. The other parameters are extracted from the charge transport measurements (SI).

In Figure 2b−e we plot the nonlocal resistance obtained from the modeling using the parameters extracted as explained above (red lines). For V_{bg} = −7.75 V there is a very good agreement between the model and the experimental values indicating the reliability of the model and the extracted parameters. As V_{bg} is reduced the agreement between the model and experimental data gets less perfect. We want to stress that such discrepancies are expected from the exponential dependence of the spin signal with the spin relaxation length in the different regions and from the presence of p−n junctions in our sample in Figure 2b,c.

Despite uncertainties, we notice that, in 2c, when the doping of the encapsulated and nonencapsulated regions has opposite sign and p−n junctions are present, even though there is a disagreement between the model and experiment in the magnitude of the modulation, the simulated signal follows the same trend as the measured data. This is achieved by taking into account the presence of regions III and V. In these regions, the drift is opposite to the one in the encapsulated regions and this explains the decrease in the nonlocal resistance at I_{dc} = −40 μA. We notice that the position of this peak is very sensitive to small uncertainties in the parameters, in particular, the spin lifetime in the outer regions.

In Figure 2b, we see that the agreement between data and experiment is not very good in either right and left detectors. We attribute this to the fact that the resistance in the nonencapsulated regions is high and the drift velocity in the outer regions increases. This makes the modeling much more sensitive to uncertainties in the parameters of both regions.

The strong modulation of the signal measured is mainly caused by an efficient modulation of the spin relaxation length. In Figure 3, we show the spin relaxation length achieved at V_{bg} = −13.75 V in the encapsulated region. We see that it increases up to 90 μm for DC currents of 90 μA (red line) when the spin

DOI: 10.1021/acs.nanolett.6b01004
Nano Lett. 2016, 16, 4825−4830

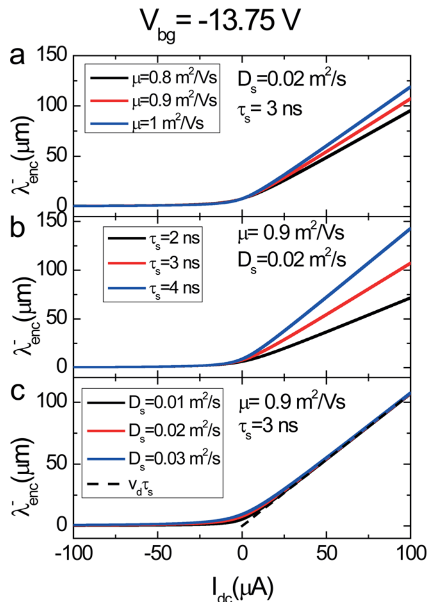

Figure 3. Extracted spin relaxation length as a function of the drift current taking into account uncertainties in the mobility (a), spin lifetime (b), and spin diffusion coefficient (c).

relaxation length at zero DC current is 7.7 μm. This observation shows the potential of drift currents to transport spins over long distances. Panels a, b, and c show the effect of our experimental uncertainties in the determination of the spin relaxation length. Because of the relevant uncertainties in the spin relaxation time, we have modeled the data at $V_{bg} = -13.75$ V for $\tau_s = 2$, 3, and 4 ns (SI). Results from this modeling show that the best agreement is achieved for $\tau_s = 4$ ns.

To account for future applications, we have also studied if it is possible to direct spins in a specific direction. We define the directionality of the spin current as $D = (J_{sL} - J_{sR})/(J_{sL} + J_{sR})$ where $J_{sR(L)}$ is the spin current toward the right (left) of the spin injector (contact 4). In Figure 4c−f, we show the I_{dc} dependence of D for our device geometry obtained from modeling at $V_{bg} = -30$, −20, −13.75, and −7.75 V.

We distinguish between two relevant cases: the ones in which the encapsulated region is hole-doped (a, c, and d) and the ones in which it is electron-doped (b, e, and f). In the first case, the drift in the encapsulated region opposes the one in the outer region (a) and the efficiency of the directional control is relatively small ((c) and (d), red lines).

When the encapsulated region is electron doped the drift has the same direction in all the regions resulting in an efficient control of the spin propagation. For instance at $V_{bg} = -13.75$ V, 88% of the spins can be directed toward the outer regions and 82% can be pulled to cross the encapsulated region by sourcing a drift current of $I_{dc} = \mp 90$ μA, respectively when, at zero drift, 66% of the spins diffuse toward the left. This asymmetry with I_{dc} is caused by the different spin transport properties of both regions. To understand this effect better, we have extracted the directionality for the case when region III is not present and the contact is placed next to the encapsulated region (Figure 4c−f black lines). In this case, when p−n junctions are present, the encapsulated region reverses the directionality modulation and makes it more efficient. When doing the same in (e), the efficiency is enhanced and 99.2% and 84% of the spins can be directed toward the left and right sides of the injector, respectively.

Such a modulation suggests that the directional control can be greatly enhanced in fully encapsulated devices and, to confirm our hypothesis, we have measured the directionality in a homogeneous device with the properties of our encapsulated region. Also, to confirm the robustness of the effect, we have calculated for both cases of $V_{bg} = -13.75$ and −7.75 V (see Figure 5). The results indicate that, in a fully encapsulated sample, 82% of the spins can be controlled with drift currents of 90 μA, whereas this number rises up to 88% for $I_{dc} = -90$ μA.

In conclusion, we have shown that the spin transport can be controlled efficiently by applying drift currents in high mobility hBN encapsulated bilayer graphene. Our results, together with a model, show that, starting from a spin relaxation length of 7.7 μm, we have achieved a strong modulation of this length from 0.6 to 90 μm when applying a drift current of ±90 μA. We notice that we cannot explore the full potential of the spin drift because the length of the graphene channel in exfoliated devices

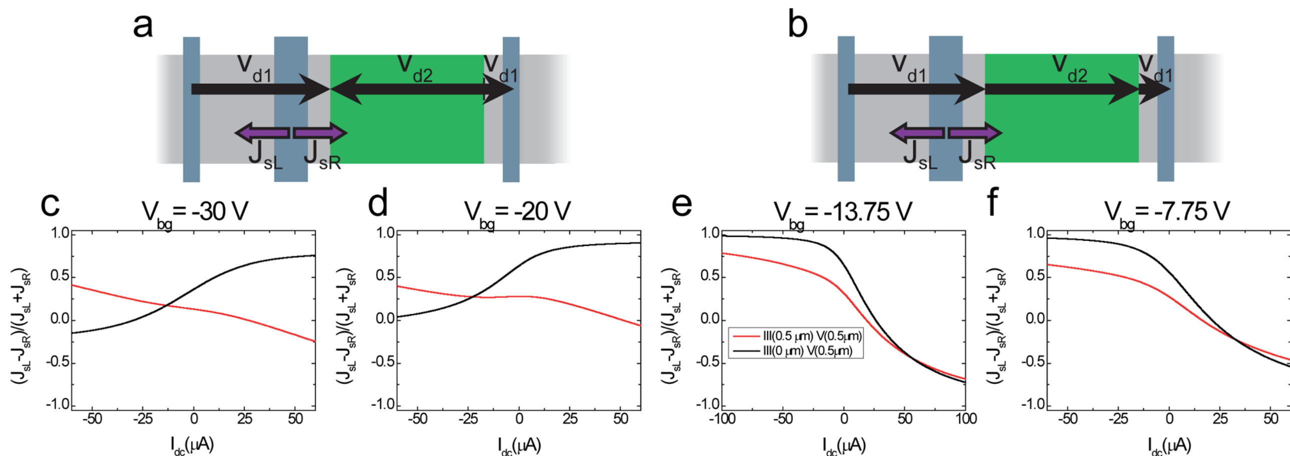

Figure 4. Directional control of spin currents. (a), (b) Injected spin currents propagating toward the left (right) side of the injector ($J_{sL(R)}$) in the modeled device geometry for the case when carriers in the encapsulated and nonencapsulated regions have the same ((b), (e), and (f)) and opposite polarity ((a), (c), and (d)). (c)−(f) Directionality of the spin currents as a function of the DC current in our device under different gating conditions. The red lines are obtained including a small nonencapsulated region between the injector contact, whereas for the black lines, these regions are removed.

DOI: 10.1021/acs.nanolett.6b01004
Nano Lett. 2016, 16, 4825−4830

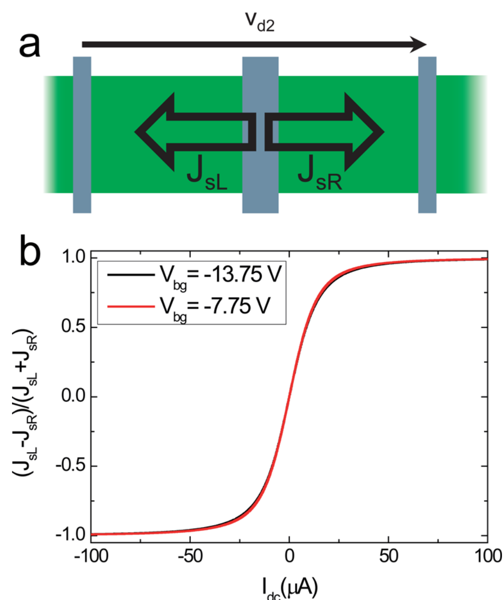

Figure 5. (a) Homogeneous geometry used to compare the results with a fully encapsulated sample where the spacing between the spin injector (4) and the contacts where I_{dc} is applied (3 and 5) is of 14.6 μm. (b) Directionality extracted for the above-mentioned geometry using the parameters obtained at V_{bg} = −13.75 and −7.75 V.

is constrained by the size of the flakes which can be obtained. Recent advances obtaining ultrahigh quality CVD graphene[30,31] make it possible to obtain high quality large devices showing spin transport over unprecedentedly long distances.

Using our model, we also extract the directionality of the spin currents. We find that, when a drift current of −90 μA is applied, 88% of the spins are directed toward the left. When applying a DC current of 90 μA 82% of the spins are directed to the right. These results show that we have achieved efficient directional control of the spin currents at room temperature. These numbers rise up to 99.4% for fully encapsulated devices, showing that the control we achieved of the directionality of the spin propagation can enable new types of spin-based logic operations. The directional control of spin currents achieved in our experiment shows that it is possible to realize logic operations using spin currents in a material with low spin orbit coupling such as graphene, opening the way to new device geometries and functionalities.

■ ASSOCIATED CONTENT

Supporting Information

The Supporting Information is available free of charge on the ACS Publications website at DOI: 10.1021/acs.nanolett.6b01004.

Device characterization, derivation of the model, and effect of τ_{enc} to the modeling. (PDF)

■ AUTHOR INFORMATION

Corresponding Author

*E-mail: J.Ingla.Aynes@rug.nl.

Notes

The authors declare no competing financial interest.

■ ACKNOWLEDGMENTS

The authors thank J. C. Leutenantsmeyer, I. J. Vera-Marun, and M. H. D. Guimarães for insightful discussions and H. Adema, J. G. Holstein, H. M. de Roosz, and T. Schouten for technical assistance. The research leading to these results has received funding from the People Programme (Marie Curie Actions) of the European Union's Seventh Framework Programme FP7/2007-2013/under REA grant agreement no. 607904-13 Spinograph and the European Union Seventh Framework Programme under grant agreement no. 604391 Graphene Flagship.

■ REFERENCES

(1) žutić, I.; Fabian, J.; Das Sarma, S. *Rev. Mod. Phys.* **2004**, *76*, 323−410.

(2) Yu, Z. G.; Flatté, M. E. *Phys. Rev. B: Condens. Matter Mater. Phys.* **2002**, *66*, 235302.

(3) Vera-Marun, I. J.; Ranjan, V.; van Wees, B. J. *Phys. Rev. B: Condens. Matter Mater. Phys.* **2011**, *84*, 241408.

(4) Appelbaum, I.; Huang, B.; Monsma, D. J. *Nature* **2007**, *447*, 295−298.

(5) Kameno, M.; Ando, Y.; Shinjo, T.; Koike, H.; Sasaki, T.; Oikawa, T.; Suzuki, T.; Shiraishi, M. *Appl. Phys. Lett.* **2014**, *104*, 092409.

(6) Sasaki, T.; Ando, Y.; Kameno, M.; Tahara, T.; Koike, H.; Oikawa, T.; Suzuki, T.; Shiraishi, M. *Phys. Rev. Appl.* **2014**, *2*, 034005.

(7) Lou, X.; Adelmann, C.; Crooker, S. A.; Garlid, E. S.; Zhang, J.; Reddy, K. S. M.; Flexner, S. D.; Palmstrøm, C. J.; Crowell, P. A. *Nat. Phys.* **2007**, *3*, 197−202.

(8) Huang, B.; Monsma, D. J.; Appelbaum, I. *Phys. Rev. Lett.* **2007**, *99*, 177209.

(9) Castro Neto, A. H.; Guinea, F.; Peres, N. M. R.; Novoselov, K. S.; Geim, A. K. *Rev. Mod. Phys.* **2009**, *81*, 109−162.

(10) Morozov, S. V.; Novoselov, K. S.; Katsnelson, M. I.; Schedin, F.; Elias, D. C.; Jaszczak, J. A.; Geim, A. K. *Phys. Rev. Lett.* **2008**, *100*, 016602.

(11) Tombros, N.; Jozsa, C.; Popinciuc, M.; Jonkman, H. T.; van Wees, B. J. *Nature* **2007**, *448*, 571.

(12) Kamalakar, M. V.; Groenveld, C.; Dankert, A.; Dash, S. P. *Nat. Commun.* **2015**, *6*, 6766.

(13) Drögeler, M.; Franzen, C.; Volmer, F.; Pohlmann, T.; Banszerus, L.; Wolter, M.; Watanabe, K.; Taniguchi, T.; Stampfer, C.; Beschoten, B. *Nano Lett.* **2016**, *16*, 3533−3539. PMID: 27210240.

(14) Roche, S.; Valenzuela, S. O. *J. Phys. D: Appl. Phys.* **2014**, *47*, 094011.

(15) Han, W.; Kawakami, R. K.; Gmitra, M.; Fabian, J. *Nat. Nanotechnol.* **2014**, *9*, 794−807.

(16) Józsa, C.; Popinciuc, M.; Tombros, N.; Jonkman, H. T.; van Wees, B. J. *Phys. Rev. Lett.* **2008**, *100*, 236603.

(17) Dean, C. R.; Young, A. F.; Meric, I.; Lee, C.; Wang, L.; Sorgenfrei, S.; Watanabe, K.; Taniguchi, T.; Kim, P.; Shepard, K. L.; Hone, J. *Nat. Nanotechnol.* **2010**, *5*, 722−726.

(18) Wang, L.; Meric, I.; Huang, P. Y.; Gao, Q.; Gao, Y.; Tran, H.; Taniguchi, T.; Watanabe, K.; Campos, L. M.; Muller, D. A.; Guo, J.; Kim, P.; Hone, J.; Shepard, K. L.; Dean, C. R. *Science* **2013**, *342*, 614−617.

(19) Guimarães, M. H. D.; Zomer, P. J.; Ingla-Aynés, J.; Brant, J. C.; Tombros, N.; van Wees, B. J. *Phys. Rev. Lett.* **2014**, *113*, 086602.

(20) Drögeler, M.; Volmer, F.; Wolter, M.; Terrés, B.; Watanabe, K.; Taniguchi, T.; Güntherodt, G.; Stampfer, C.; Beschoten, B. *Nano Lett.* **2014**, *14*, 6050−6055. PMID: 25291305.

(21) Ingla-Aynés, J.; Guimarães, M. H. D.; Meijerink, R. J.; Zomer, P. J.; van Wees, B. J. *Phys. Rev. B: Condens. Matter Mater. Phys.* **2015**, *92*, 201410.

(22) Avsar, A.; Vera-Marun, I. J.; Tan, J. Y.; Koon, G. K. W.; Watanabe, K.; Taniguchi, T.; Adam, S.; Ozyilmaz, B. *NPG Asia Mater.* **2016**, *8*, e274.10.1038/am.2016.65

(23) Zomer, P. J.; Guimarães, M. H. D.; Brant, J. C.; Tombros, N.; van Wees, B. J. *Appl. Phys. Lett.* **2014**, *105*, 013101.

DOI: 10.1021/acs.nanolett.6b01004
Nano Lett. 2016, 16, 4825−4830

(24) In ref 32, the effect of drift induced by a bias current though a contact on the spin injection efficiency has been studied. In our case, there is no current bias through the spin injector/detector contacts, and the spin injection/detection efficiency is assumed constant. For the sake of completeness, we have also carried out the mentioned experiments in our device and measured modulations of the spin signal up to ± 10% when applying drift currents up to ± 40 μA.
(25) Evolution of the switches with drift confirm that the switches are created by contact 4 and not by 3.
(26) Novoselov, K. S.; Geim, A. K.; Morozov, S. V.; Jiang, D.; Zhang, Y.; Dubonos, S. V.; Grigorieva, I. V.; Firsov, A. A. *Science* **2004**, *306*, 666−669.
(27) We notice that R_{nl}^{L} in Figure 2b,e at zero drift current is higher than in Figure 2c,d. This is because the data in Figure 2b,e are obtained in a slightly different geometry with a small shift of contact 3.
(28) Popinciuc, M.; Józsa, C.; Zomer, P. J.; Tombros, N.; Veligura, A.; Jonkman, H. T.; van Wees, B. J. *Phys. Rev. B: Condens. Matter Mater. Phys.* **2009**, *80*, 214427.
(29) Guimarães, M. H. D.; Veligura, A.; Zomer, P. J.; Maassen, T.; Vera-Marun, I. J.; Tombros, N.; van Wees, B. J. *Nano Lett.* **2012**, *12*, 3512−3517. PMID: 22709361.
(30) Banszerus, L.; Schmitz, M.; Engels, S.; Dauber, J.; Oellers, M.; Haupt, F.; Watanabe, K.; Taniguchi, T.; Beschoten, B.; Stampfer, C. *Science Advances* **2015**, *1*, e1500222.
(31) Banszerus, L.; Schmitz, M.; Engels, S.; Goldsche, M.; Watanabe, K.; Taniguchi, T.; Beschoten, B.; Stampfer, C. *Nano Lett.* **2016**, *16*, 1387−1391. PMID: 26761190.
(32) Józsa, C.; Popinciuc, M.; Tombros, N.; Jonkman, H. T.; van Wees, B. J. *Phys. Rev. B: Condens. Matter Mater. Phys.* **2009**, *79*, 081402.

DOI: 10.1021/acs.nanolett.6b01004
Nano Lett. 2016, 16, 4825−4830